European Conference on Computational Fluid Dynamics
ECCOMAS CFD 2006
P. Wesseling, E. Oñate and J. Périaux (Eds)

REGULARIZATION MODELS FOR THE SIMULATION OF TURBULENCE IN A DIFFERENTIALLY HEATED CAVITY

F.X. Trias*, M. Soria*, A. Oliva* and R.W.C.P. Verstappen*

* Centre Tecnològic de Transferència de Calor, Universitat Politènica de Catalunya
C/Colom, 11 08222 Terrassa, Barcelona, Spain, E-mail: cttc@cttc.upc.edu
* Institute of Mathematics and Computing Science, University of Groningen
P.O. Box 800, 9700 AV Groningen, The Netherlands, E-mail: R.W.C.P.Verstappen@rug.nl

Key words: Turbulent heat transfer, turbulence modelling, symmetry and conservation

Abstract. *Since direct numerical simulations (DNS) of natural convection in a differentially heated cavity can not be performed at high Ra-numbers, a dynamically less complex mathematical formulation is sought. In the quest for such a formulation, we consider regularizations (smooth approximations) of the nonlinearity. The regularization method basically alters the convective terms to reduce the production of small scales of motion by means of vortex stretching. In doing so, we propose to preserve the symmetry and conservation properties of the convective terms exactly. This requirement yields a novel class of regularizations that restrain the convective production of smaller and smaller scales of motion by means of vortex stretching in an unconditional stable manner, meaning that the velocity can not blow up in the energy-norm (in 2D also: enstrophy-norm). The numerical algorithm used to solve the governing equations preserves the symmetry and conservation properties too. The regularization model is successfully tested for a 3D natural convection flow in a differentially heated cavity ($Ra = 10^{10}$, $Pr = 0.71$ and height aspect ratio 4)*

1 INTRODUCTION

Natural convection in parallelepipedic enclosures has been the subject of numerous studies over the past decades. Most of them can be classified in three main groups: cavities where the flow is due to internal heat generation, cavities heated from below (Rayleigh-Bénard configuration), and those heated from the sides. The configuration of the latter class is the differentially heated cavity, the situation that here is under consideration. This models many engineering applications such as ventilation of rooms, cooling of electronics devices or air flow in buildings. Simultaneously, this configuration has served as prototype for the development of numerical algorithms.

An accurate prediction of the flow structure and the heat transfer in such configuration is of great interest and despite the great effort devoted (see for instance [1, 2, 3]) for an accurate turbulence modelling of this configuration it remains as a great challenge. This

is mainly due to the complex behaviour exhibit: the boundary layers remain laminar in their upstream part up to the point where the waves travelling downstream grow up enough to disrupt the boundary layers ejecting large unsteady eddies to the core of the cavity. The mixing effect of these eddies, that throw hot and cold fluid respectively, tends to result in almost isothermal hot upper and cold lower regions. This mixing effect at the top and bottom areas of the cavity, force the temperature drop in the core of the cavity occurs in a smaller region. Moreover, recently important differences have been observed between 2D and 3D configurations [4, 5]. In the 3D DNS simulations these large eddies do not persist and its energy is rapidly passed down the cascade to smaller eddies. It yields on a manifest reduction of the mixing effect at the hot upper and cold lower regions and consequently a still motionless stratified cavity core. The cavity core remains still almost motionless and very well stratified in an evident contrast with the 2D simulation results that display increasingly large top and bottom regions of disorganisation that consequently reduce the area of uniform temperature stratification. These differences between 2D and 3D turbulence flow dynamics are clearly observed in the time sequences of isotherms displayed in the figure 1.

At high Ra-numbers, the 3D dynamics can not be studied since DNS's are not feasible. Therefore, a dynamically less complex mathematical formulation is sought. In the quest for such a formulation, we consider regularizations (smooth approximations) of the nonlinearity. The proposed regularization method basically alters the convective terms to reduce the production of small scales of motion in an unconditional stable manner. In this paper, a direct comparison between 3D DNS results [5] at $Ra = 10^{10}$ and numerical results obtained with the regularization model is carried out. The paper is organised as follows. In Section 2, the regularization model is described. In Section 3, the performance of the regularization model is evaluated by means of direct comparison with reference DNS data. Finally, the results are summarised and conclusions are given in Section 4.

2 GOVERNING EQUATIONS AND NUMERICAL METHOD

We consider a differentially heated cavity of height aspect ratio 4 filled with an incompressible fluid. The Rayleigh number Ra based on the cavity height is $(g\beta\Delta T L_z^3)/(\nu\alpha)$, and the Prandlt number $Pr = \nu/\alpha$ is 0.71 (air). To account for density variations, the Boussinesq approximation is used. Thermal radiation is neglected. Under these conditions, the velocity u and the temperature T are governed by the following set of partial differential equations

$$\partial_t u + \mathcal{C}(u,u) = \frac{Pr}{\sqrt{Ra}}\Delta u - \nabla p + f, \tag{1}$$

$$\partial_t T + \mathcal{C}(u,T) = \frac{1}{\sqrt{Ra}}\Delta T, \tag{2}$$

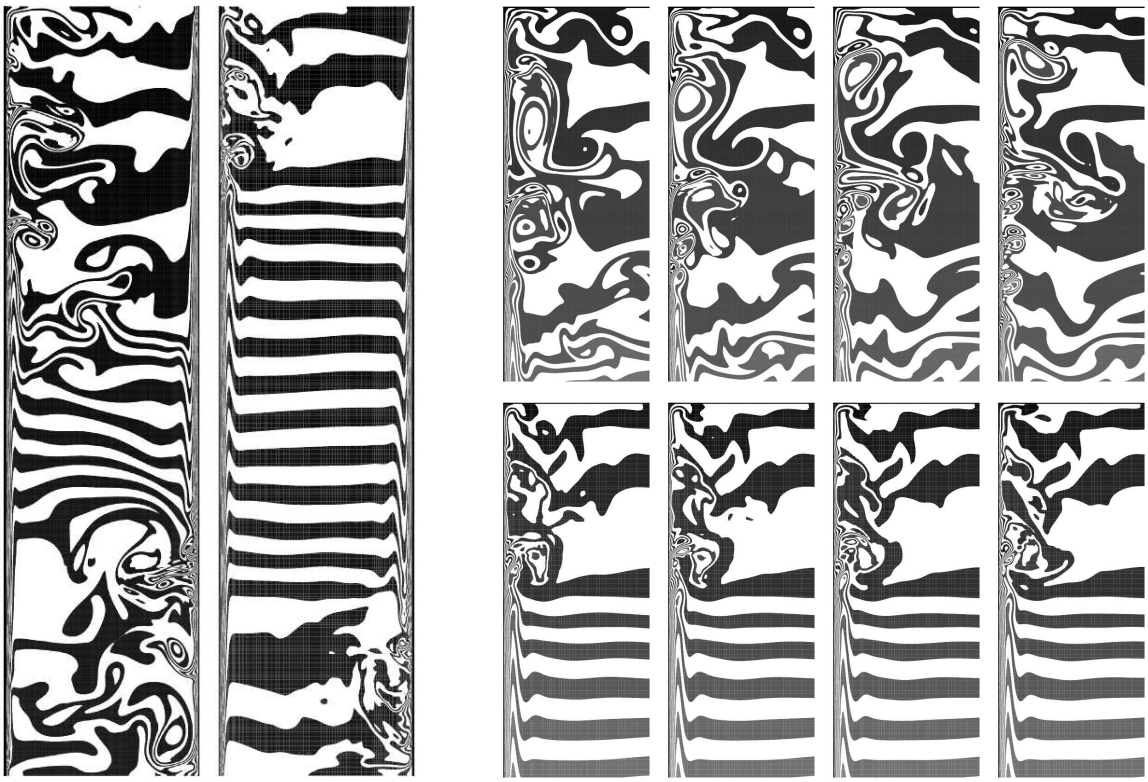

Figure 1: Left: Instantaneous isotherms at $Ra = 10^{10}$ for 2D (left) and 3D (right) DNS simulations. Right: Zoom around the top left corner of a time sequence of instantaneous isotherms for 2D (top) and 3D (bottom).

where the convective term is given by

$$\mathcal{C}(u, v) = (u \cdot \nabla)v, \tag{3}$$

the body force vector is given by $f = (0, 0, PrT)$ and the incompressibility constraint reads $\nabla \cdot u = 0$.

2.1 Regularization modelling

At high Ra-numbers, the velocity and temperature can not be computed numerically from Eqs. (1)-(2), because the solution possesses far too many scales of motion. The computationally almost numberless small scales result from the nonlinear, convective terms $\mathcal{C}(u, u)$ and $\mathcal{C}(u, T)$ that allow for the transfer of energy from scales as large as the flow domain to the smallest scales that can survive viscous dissipation. In the quest for a dynamically less complex mathematical formulation, we consider smooth approximations (regularizations) of the nonlinearity,

$$\partial_t u_\epsilon + \widetilde{C}(u_\epsilon, u_\epsilon) \;=\; \frac{Pr}{\sqrt{Ra}} \Delta u_\epsilon - \nabla p_\epsilon + f, \tag{4}$$

$$\partial_t T_\epsilon + \widetilde{\mathcal{C}}(u_\epsilon, T_\epsilon) = \frac{1}{\sqrt{Ra}} \Delta T_\epsilon, \tag{5}$$

where the variable names are changed from u and T to u_ϵ and T_ϵ, respectively, to stress that the solution of (4)-(5) differs from that of Eqs. (1)-(2).

The regularized system (4)-(5) should be more amenable to solve numerically (that is, the regularization should limit the production of small scales of motion), while the leading modes of u_ϵ, T_ϵ have to approximate the corresponding modes of the solution u, T of Eqs. (1)-(2) .

The first outstanding approach in this direction goes back to Leray [6], who took $\widetilde{C}(u,u) = C(\bar{u},u)$ and proved that a moderate filtering of the transport velocity is sufficient to regularize a turbulent flow. Here, the filtering operation is denoted by a bar. The Navier-Stokes-α-model forms another example of regularization modelling [7]. In this model, the convective term becomes $\widetilde{C}_r(u,u) = C_r(u,\bar{u})$, where C_r denotes the convective operator in rotational form: $C_r(u,v) = (\nabla \times u) \times v$.

The regularization given by (4)-(5) may also seen in relation to large-eddy simulation (LES). In LES, Eqs. (1)-(2) are filtered spatially, and the resulting nonlinear terms involving residual velocities and temperatures are modelled in terms of the filtered velocity and temperature fields:

$$\partial_t \overline{u}_\epsilon + \mathcal{C}(\overline{u}_\epsilon, \overline{u}_\epsilon) = \frac{Pr}{\sqrt{Ra}} \Delta u_\epsilon - \nabla p_\epsilon + f + \mathcal{M}_1(\overline{u}_\epsilon), \tag{6}$$

$$\partial_t \overline{T}_\epsilon + \widetilde{\mathcal{C}}(\overline{u}_\epsilon, \overline{T}_\epsilon) = \frac{1}{\sqrt{Ra}} \Delta \overline{T}_\epsilon + \mathcal{M}_2(\overline{u}_\epsilon, \overline{T}_\epsilon), \tag{7}$$

where the model terms are approximately given by

$$\mathcal{M}_1(\overline{u}_\epsilon) \approx \mathcal{C}(\overline{u}_\epsilon, \overline{u}_\epsilon) - \overline{\mathcal{C}(u_\epsilon, u_\epsilon)}, \qquad \mathcal{M}_2(\overline{u}_\epsilon, \overline{T}_\epsilon) \approx \mathcal{C}(\overline{u}_\epsilon, \overline{T}_\epsilon) - \overline{\mathcal{C}(u_\epsilon, T_\epsilon)}.$$

The regularization described by Eqs. (4)-(5) falls in with this concept if

$$\overline{\widetilde{C}(u_\epsilon, u_\epsilon)} = C(\overline{u}_\epsilon, \overline{u}_\epsilon) - \mathcal{M}_1(\overline{u}_\epsilon), \qquad \overline{\widetilde{C}(u_\epsilon, T_\epsilon)} = C(\overline{u}_\epsilon, \overline{T}_\epsilon) - \mathcal{M}_2(\overline{u}_\epsilon, \overline{T}_\epsilon). \tag{8}$$

Indeed under this condition, Eqs. (4)-(5) are equivalent to (6)-(7): we can filter (4)-(5) first and thereafter compare the filtered version of (4) -(5) term-by-term with (6)-(7) to identify the closure models $\mathcal{M}_1(\overline{u}_\epsilon)$ and $\mathcal{M}_2(\overline{u}_\epsilon, \overline{T}_\epsilon)$. Finally, it may be noted that Eq. (8) relates the regularization $\widetilde{C}(u_\epsilon, u_\epsilon)$ one-to-one to the closure models $\mathcal{M}_1$ and $\mathcal{M}_2$ for any invertible filter (the Gaussian filter, for instance).

2.2 Symmetry and conservation

The regularization method basically alters the nonlinearity to restrain the production of small scales of motion, see e.g. [8]-[9]. In doing so, one can preserve certain fundamental

properties of the convective operator $\mathcal{C}$ in Eqs.(1)-(2) exactly. We propose to preserve the symmetry properties that form the basis for the conservation of energy, enstrophy (in 2D) and helicity. To sketch the symmetry and conservation properties, we define the energy of a fluid with velocity u and occupying the flow domain V by $|u|^2 = (u, u)$, where $(u, v) = \int_V u \cdot v dx$ denotes the usual scalar product. The norm of the temperature becomes $|T|^2 = (T, T)$. The enstrophy is defined as $|\nabla \times u|^2$ and the helicity is given by $(\nabla \times u, u)$.

The evolution of the energy follows from differentiating (u, u) with respect to time and rewriting $\partial_t u$ with the help of (1). In this way, we get a convective contribution given by $(\mathcal{C}(u, u), u)$. This term cancels, because the trilinear form $(\mathcal{C}(u, v), w)$ is skew-symmetric with respect to v and w:

$$(\mathcal{C}(u, v), w) = -(v, \mathcal{C}(u, w)), \tag{9}$$

see e.g. [10].

Note that contributions resulting from boundary conditions are ignored here.

The same reasoning applies to dynamics of $|T|^2$: the convective contribution $(\mathcal{C}(u, T), T)$ cancels because of (9). The evolution of the enstrophy is obtained by taking the inner product of the Navier-Stokes equations with the vector field $-\Delta u$. The resulting convective contribution vanishes in two spatial dimension, since in 2D, we have [11]

$$(\mathcal{C}(u, v), \Delta v) = (u, \mathcal{C}(\Delta v, v)), \tag{10}$$

where the right-hand side vanishes for $u = v$ because of (9). The evolution of the helicity follows from the inner product of Eq. (1) with the vorticity $\omega = \nabla \times u$ and the inner product of the curl of Eq. (1) with the velocity u. Taking these inner products results into the convective contribution $(\mathcal{C}(u, u), \omega) + (\mathcal{C}(u, \omega), u) - (\mathcal{C}(\omega, u), u)$, which vanishes as an immediate consequence of the skew symmetry (9). Therefore, the helicity is conserved in the absence of viscous dissipation.

2.3 Symmetry-preserving regularization models

We aim to regularize the convective operator $\mathcal{C}$ in such manner that the underlying symmetries (given by Eq. (9) and Eq. (10)) are preserved. In other words, we require that the approximation $\widetilde{\mathcal{C}}$ of $\mathcal{C}$ satisfies

$$(\widetilde{\mathcal{C}}(u, v), w) = -(v, \widetilde{\mathcal{C}}(u, w)), \tag{11}$$

and in 2D,

$$(\widetilde{\mathcal{C}}(u, v), \Delta v) = (u, \widetilde{\mathcal{C}}(\Delta v, v)). \tag{12}$$

This criterion yields the following class of regularizations

$$\widetilde{\mathcal{C}}_2(u,v) = \overline{\mathcal{C}(\overline{u},\overline{v})} \quad (13)$$
$$\widetilde{\mathcal{C}}_4(u,v) = \mathcal{C}(\overline{u},\overline{v}) + \overline{\mathcal{C}(\overline{u},v')} + \overline{\mathcal{C}(u',\overline{v})} \quad (14)$$
$$\widetilde{\mathcal{C}}_6(u,v) = \mathcal{C}(\overline{u},\overline{v}) + \mathcal{C}(\overline{u},v') + \mathcal{C}(u',\overline{v}) + \overline{\mathcal{C}(u',v')}, \quad (15)$$

where a prime indicates the residual of the filter, *e.g.* $u' = u - \overline{u}$. The difference between $\widetilde{C}_n(u,u)$ and $C(u,u)$ is of the order ϵ^n (where n=2,4,6) for symmetric filters with filter length ϵ. Note that for a generic, symmetric filter: $u' = \mathcal{O}(\epsilon^2)u$, cf. [12].

The transport theorem (see *e.g.* [13]) states that for any part W of the fluid domain, we have

$$\frac{\mathrm{d}}{\mathrm{d}t}\int_W v \mathrm{d}W = \int_W \frac{\partial v}{\partial t}\mathrm{d}W + \int_{\partial W} v\, u\cdot n \mathrm{d}S = \int_W \left(\frac{\partial v}{\partial t} + \mathcal{C}(u,v)\right)\mathrm{d}W,$$

where the last equality follows from the divergence theorem of Gauss (provided $\nabla\cdot u = 0$). In view of this, the approximation $\mathcal{C}_n(u,v)$ of $\mathcal{C}(u,v)$ may be derived by smoothing the flux through the boundary ∂W of W. For instance, the approximation $\mathcal{C}_4$ is found if $v\, u\cdot n$ is replaced by $(\overline{v}\,\overline{u} + \overline{\overline{v}\,u'} + \overline{v'\,\overline{u}})\cdot n$.

The approximations $\widetilde{C}_n(u_\epsilon,u_\epsilon)$ are stable by construction, meaning that no convective terms contribute to the evolution of $|u_\epsilon|^2$ and $|T_\epsilon|^2$; hence, the evolution of both $|u_\epsilon|^2$ and $|T_\epsilon|^2$ is governed by a dissipative process.

2.4 Nonlinear transport mechanism

To see how the above regularizations restrain the production of small scales of motion, we take the curl of Eq. (4), with $\widetilde{C}$ as in Eqs. (13)-(15),

$$\partial_t\omega_\epsilon + \widetilde{\mathcal{C}}_n(u_\epsilon,\omega_\epsilon) = \frac{Pr}{\sqrt{Ra}}\Delta\omega_\epsilon + \nabla\times f + \widetilde{\mathcal{C}}_n(\omega_\epsilon,u_\epsilon). \quad (16)$$

This equation resembles the vorticity equation that results from the Navier-Stokes equations: the only difference is that $\mathcal{C}$ is replaced by its regularization $\widetilde{\mathcal{C}}_n$. If it happens that the vortex stretching term $\mathcal{C}_n(\omega_\epsilon,u_\epsilon)$ in Eq. (16) is so strong that the dissipative term $(Pr/Ra)\Delta\omega_\epsilon$ can not prevent the intensification of vorticity, smaller vortical structures are produced. The Navier-Stokes equations lead to the source term

$$\mathcal{C}(\omega,u) = S\omega = \overline{S}\overline{\omega} + \overline{S}\omega' + S'\overline{\omega} + S'\omega', \quad (17)$$

where $S = \frac{1}{2}(\nabla u + \nabla u^{\mathrm{T}})$ is the deformation tensor. The regularization reduce the high frequencies in the vortex stretching term:

$$\widetilde{\mathcal{C}}_2(\omega,u) = \overline{\overline{S}\overline{\omega}}$$
$$\widetilde{\mathcal{C}}_4(\omega,u) = \overline{S}\overline{\omega} + \overline{\overline{S}\omega'} + \overline{S'\overline{\omega}}$$
$$\widetilde{\mathcal{C}}_6(\omega,u) = \overline{S}\overline{\omega} + \overline{S}\omega' + S'\overline{\omega} + \overline{S'\omega'}$$

Qualitatively, vortex stretching leads to the production of smaller and smaller scales, *i.e.*, to a continuous, local increase of both S' and ω'. Consequently, at the positions where vortex stretching occurs, the terms with S' and ω' will eventually amount considerably to $\mathcal{C}(\omega, u)$. Since the regularizations $\widetilde{\mathcal{C}}_n(\omega, u)$ diminish these terms, they counteract the production of smaller and smaller scales by means of vortex stretching and may eventually stop the continuation of the vortex stretching process. In this way, the symmetry-preserving regularization method restrains the convective production of smaller and smaller scales of motion by means of vortex stretching, while ensuring that convection makes no contribution to the dynamics of both $|u_\epsilon|^2$ and $|T_\epsilon|^2$.

A detailed study of the triadic interactions shows that $\widetilde{\mathcal{C}}_n(u, u)$ approximates the local interactions between large scales of motion ($\epsilon|k| < 1$) up to n-th order. Hence, the triadic interactions between large scales are only slightly altered. All interactions involving longer wavevectors (smaller scales of motion) are reduced. The amount by which the interactions between the wavevector-triple (k, p, q) are lessened depends on the length of the legs of the triangle $k = p + q$. In case $n = 4$, for example, all triadic interactions for which at least two legs are (much) longer than $1/\epsilon$ are (strongly) attenuated, whereas interactions for which at least two legs are (much) shorter than $1/\epsilon$ are reduced to a small degree only.

2.5 Choice of the filter

The filter is based upon the elliptic differential operator,

$$(1 - \partial_i \alpha_i \partial_i)\, \overline{u} = u, \tag{18}$$

where the coefficients α_1, α_2 and α_3 parameterize the length of the filter in the x_1-, x_2- and x_3-direction. Note that Eq.(18) reduces to the Helmholtz filter in the isotropic case: $\alpha_i = \alpha$. The filter length is defined by $\epsilon = \alpha\sqrt{24}$, *i.e.*, need not be restricted to integer multiples of the grid width. The boundary conditions that supplement the Navier-Stokes equations are also applied to (18). The filter (18) commutes with the gradient operator, that is $\overline{\nabla\phi} = \nabla\overline{\phi}$ for any (sufficiently differentiable) scalar ϕ. This implies that the approximations $\mathcal{C}_n$ are exact for potential flows. More importantly, if we decompose the velocity field u into a gradient part and a rotational part, $u = \nabla\phi + \nabla\times\Psi$, we see that the fluctuating part u' of u is purely rotational: $u' = \nabla \times \Psi'$. Thus, the fluctuating velocity captures a characteristic property of turbulence: it consists of fluctuating rotational flow. The filter given by Eq. (18) is generic in the sense that any symmetric convolution filter can be approximated by the diffusive process (18), where the error in the approximation is of the order α^4 [12].

Since solving the Helmholtz equation for $\overline{u}$ is rather expensive, we have tried to reduce the filtering costs by truncating the iterative solution method for (18) numerically before the point of convergence is approached. In doing so, we found that one Jacobi iteration (with $\overline{u} = u$ as initial guess) suffice already. Therefore, the results shown in Section 3 are obtained by means of one Jacobi iteration.

	DNS	RM1	RM2
Nx	64	8	8
Ny	136	17	13
Nz	324	40	30
Δx_{min}	7.81×10^{-3}	6.25×10^{-2}	6.25×10^{-2}
Δy_{min}	1.11×10^{-3}	8.88×10^{-3}	1.16×10^{-2}
Δz_{min}	1.23×10^{-2}	9.96×10^{-2}	1.33×10^{-1}

Table 1: Description of meshes.

2.6 Numerical method

To evaluate the performance of the proposed regularization models, numerical results are compared with reference data in Section 3. In such an *a posteriori* test modelling errors and discretization errors are mixed together. Consequently, the discretization of the governing equations is a very important point when dealing with *a posteriori* performance tests for LES-models [14]. The regularizations $\mathcal{C}_n$ given by Eqs. (13)-(15) are constructed such that symmetry properties (11) and (12) are preserved. Of course, the same should hold for the numerical approximations that are used to discretize $\mathcal{C}_n$. Therefore, we have developed a spatial discretization that preserves these properties. For a detailed explanation, the reader is referred to [15].

3 RESULTS FOR A DIFFERENTIALLY HEATED CAVITY

The performance of the symmetry-preserving regularization model C_4 is tested for a $3D$ air-filled ($Pr = 0.71$) differentially heated cavity of height aspect ratio 4 and $Ra = 10^{10}$ by means of direct comparison with our 3D DNS results [5]. We have considered two coarse meshes consisting of $8 \times 13 \times 30$ and $8 \times 17 \times 40$ grid points, respectively (see table 1). Coarse meshes $RM1$ and $RM2$ are constructed trying to maintain the same grid points distribution of the DNS but with much less spatial resolutions. For more numerical details (grid-streching, explicit time-integration method, Poisson solver, etc.) the reader is referred to [4, 5]. Of course, domain size and mesh concentration parameters are taken equal to those used for the DNS simulation.

An accurate prediction of these flows that display both laminar and turbulent zones lies on its ability to locate correctly the transitional zones. Comparison between 2D and 3D DNS results suggests [5] that this feature is intimately tied up with the capability of the convective operator to mimic correctly the physics of the original Navier-Stokes equations. Therefore, approximations of the convective operator in such a manner that the underlying symmetries and certain fundamental properties such as the inviscid invariants - kinetic energy, enstrophy (in 2D) and helicity (in 3D) - are preserved exactly even for very coarse meshes may be the key ingredient of turbulence modelling.

In the present tests, the coefficients α_i of the filter (18) are taken such that the corre-

sponding filter length $\epsilon_i = \alpha_i\sqrt{24}$ in the i-th spatial direction be equal to $\epsilon_i = rh_i$, where the ratio r does not depend on the coordinate direction and h_i denotes the average grid spacing in x_i direction. Since this ratio is chosen equal in all three spatial directions, the approximation C_4 contains only one parameter, the ratio ϵ/h (filter length to the grid width).

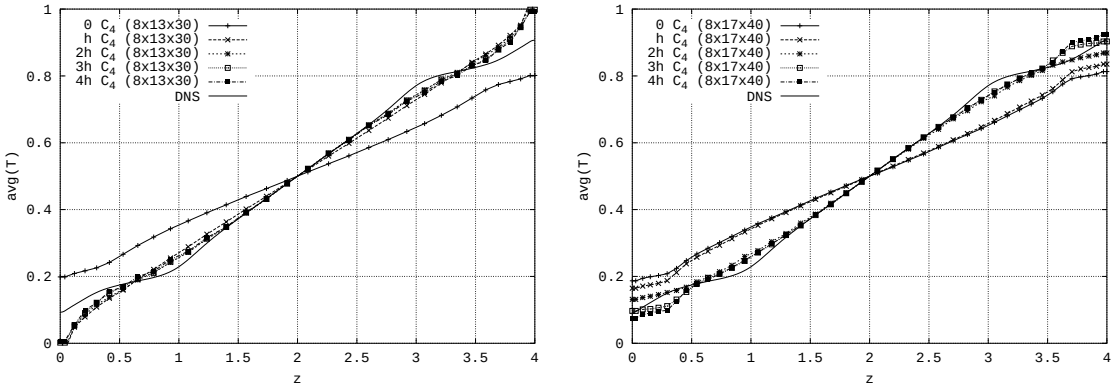

Figure 2: Averaged vertical temperature profile at mid-width for different filter lengths ϵ. Left: $8\times13\times30$ simulations. Right: $8 \times 17 \times 40$ simulations. The ratio ϵ/h (filter length to the grid width) varies from zero to four.

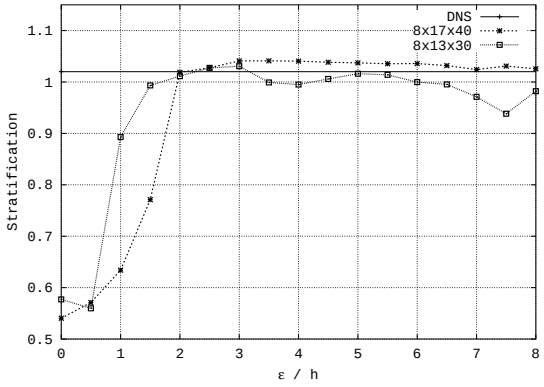

Figure 3: Dimensionless stratification in the core of the cavity as a function of the ratio of the filter length ϵ to the average grid width h

3.1 Mean fields

Averages over the three statistically invariant transformations (time, x_1-direction and central point symmetry around the centre of the cavity) have been carried out for all fields. The corresponding vertical temperature profile at mid-width is displayed in figure 2. As was pointed out in Section 1, an accurate prediction of thermal stratification is a challenge for turbulence modelling. This is due to the high sensitivity exhibit: small disturbances in

the location of the transitional point at the vertical boundary layers or a sudden 'artificial' stop of the energy cascade at large scales of motion can dramatically affect the structure of the stratified cavity core.

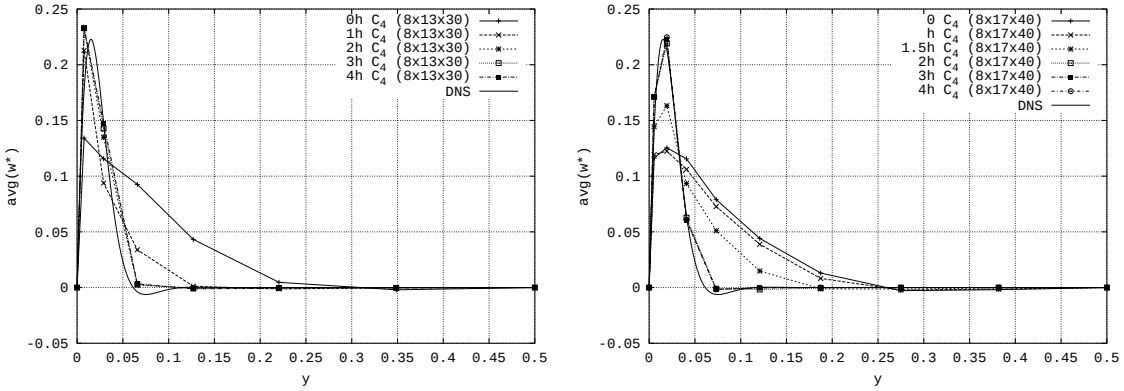

Figure 4: Averaged vertical velocity profile at the horizontal mid-height plane for different ϵ/h ratios. Left: $8 \times 13 \times 30$ simulations. Right: $8 \times 17 \times 40$ simulations

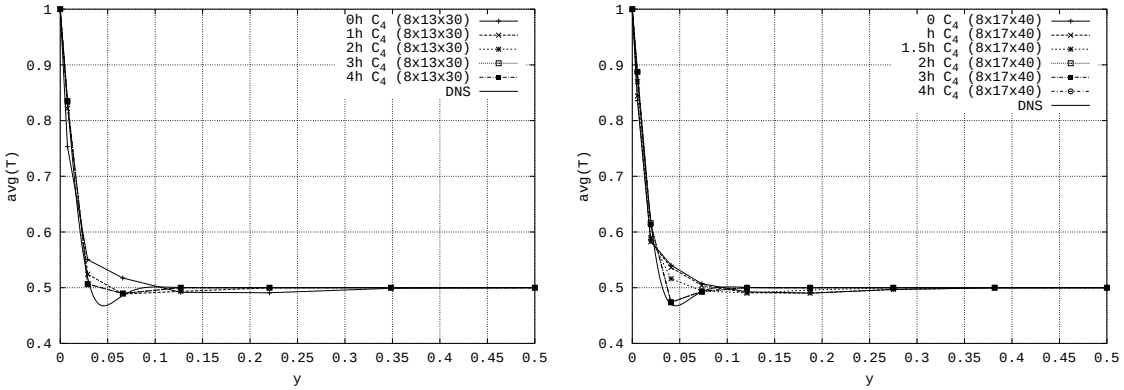

Figure 5: Averaged temperature profile at the horizontal mid-height plane for different filter lengths. Left: $8 \times 13 \times 30$ simulations. Right: $8 \times 17 \times 40$ simulations

In figures 2 and 3, we can see that without smoothing ($\epsilon = 0$), the thermal stratification in clearly underpredicted. For both coarse grids optimal values of the ratio ϵ/h are around 2.5 (see figure 3). For the finer RM1 mesh the stratification value remain almost constant for a wide range of ϵ/h whereas for the coarser moderate oscillations around the reference value are observed.

Let us now focus on the vertical boundary layer. The temperature and vertical velocity profiles are displayed in figures 4 and 5. We can see that the corresponding solutions for $\epsilon = 0$ displays a much too thick vertical boundary layer. With enough smoothing (ϵ/h ratio ≈ 3 for the RM2 grid, and ≈ 2 for the RM1 grid) the results agree very well with the

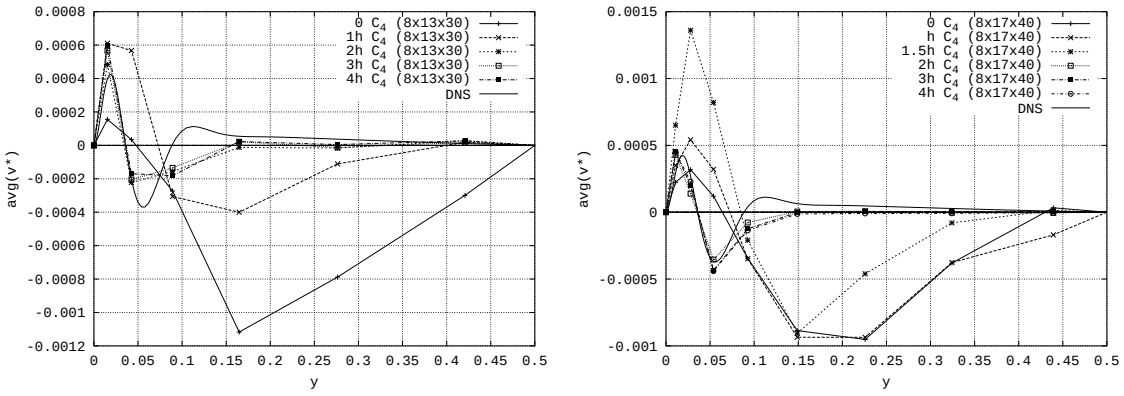

Figure 6: Averaged horizontal velocity profile at the horizontal mid-height plane for different filter lengths ϵ. Left: $8 \times 13 \times 30$ simulations. Right: $8 \times 17 \times 40$ simulations

DNS reference solution. Figure 6 depicts essentially the same for the horizontal velocity profile.

In the figure 7, the dependence of the maximum of the averaged vertical velocity at mid-height of the cavity with respect ϵ/h is analyzed. We can see that the calculations carried out with the RM1 grid predict the reference value well if the ratio ϵ/h is taken equal to ≈ 3. For the RM2 grid, the optimal ratio is about 2. In any case, the results obtained remains almost constant when the value of the filter length is increased.

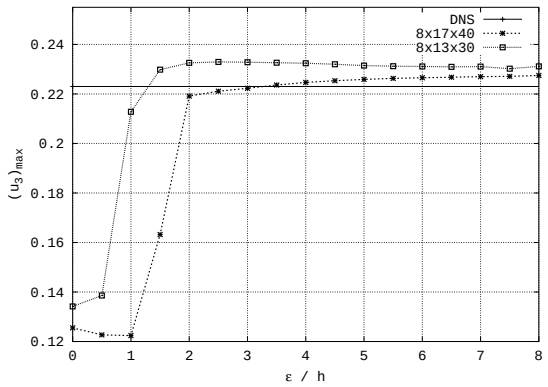

Figure 7: The maximum of the averaged vertical velocity at the horizontal mid-height plane as a function of the ratio of the filter length ϵ to the average grid width h

3.2 Heat transfer

Figure 8 displays the total Nusselt number as function of ϵ/h. The reference value $Nu = 101.70$ has been obtained from our DNS simulation (see table 1) and $\epsilon = 0$. We see that the RM1 simulations predict fairly well the reference value if the ratio ϵ/h is equal to ≈ 2. For the coarsest mesh, $8 \times 13 \times 30$, the optimal ratio ϵ/h is about 1.5 (or greater),

and, as expected, the results obtained are slightly worse. In conclusion, for both cases we observe that the solution without smoothing ($\epsilon = 0$) is incomparably worse and that similar results are again obtained for a wide range of ϵ/h values.

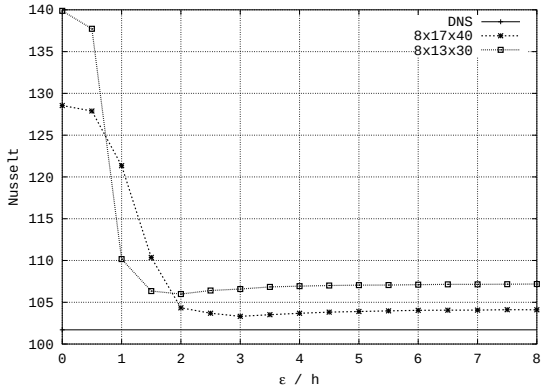

Figure 8: The overall averaged Nusselt number as a function of the ratio of the filter length ϵ to the average grid width h

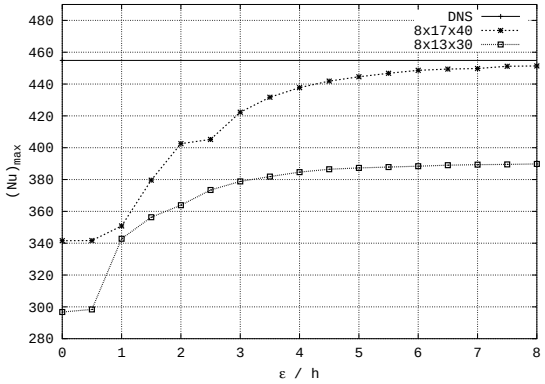

Figure 9: The maximum of the averaged Nusselt number as a function of the ratio of the filter length ϵ to the average grid width h

In the figures 9 and 10, the maximum and the mininum values of local Nusselt number as a function of ϵ/h are displayed, respectively. These two quantities are of interest because they occur in two clearly different parts of the vertical boundary layers. Maximum values occur in the upstream part of the boundary layer where it is still almost laminar whereas minimum values are observed at the most downstream part of the boundary layer where it has become fully turbulent (see figure 1, left). For both coarse grids, the optimal values of the ratio ϵ/h are about 4 (or greater).

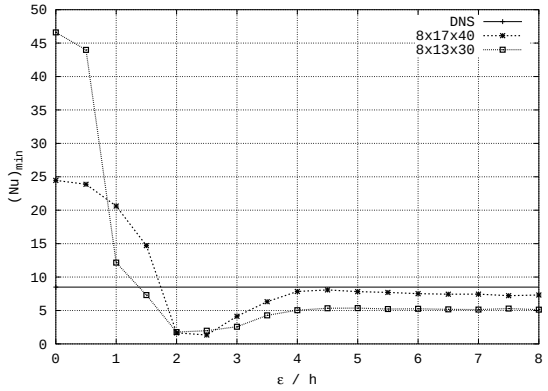

Figure 10: The minimum of the averaged Nusselt number as a function of the ratio of the filter length ϵ to the average grid width h

3.3 Turbulent statistics

Horizontal profiles at the mid-height plane of the turbulent kinetic energy, $k = \overline{u_i' u_i'}$, the temperature variance, $\overline{T'T'}$, and the turbulent heat flux, $\overline{u_3' T'}$, have been represented in figures 11, 12 and 13, respectively. An accurate prediction of turbulent quantities at this part of the vertical boundary layer is rather difficult because it is located in an area of transition from the laminar upstream to the turbulent downstream part.

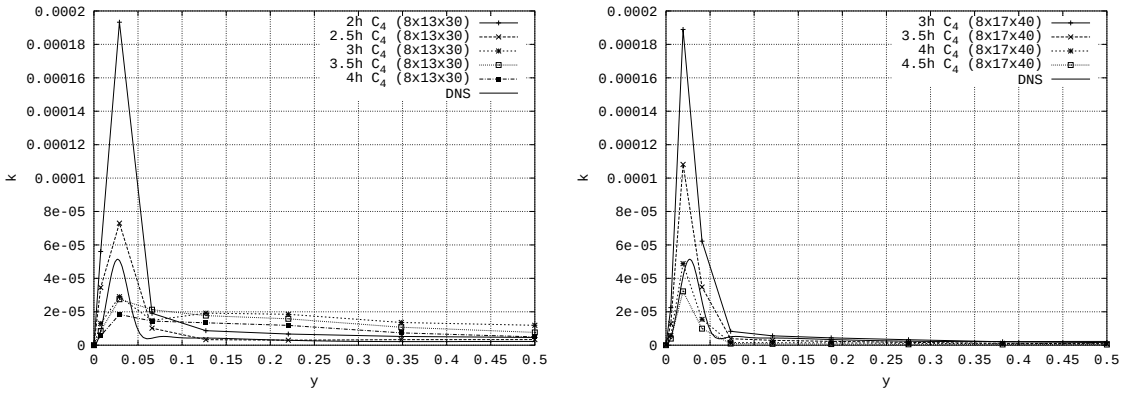

Figure 11: Turbulent kinetic energy $k = \overline{u_i' u_i'}$ profile at the horizontal mid-height plane for different filter lengths ϵ. Left: $8 \times 13 \times 30$ simulations. Right: $8 \times 17 \times 40$ simulations

At first sight we observe, that although the absolute levels are not always well predicted, the smoothed results are in fairly good agreement with the reference solution. Non-smoothed solutions ($\epsilon = 0$, not displayed here) differ from the DNS solution in several orders of magnitude for both coarse grids. It is also observed that for a relatively short range of ϵ/h ratios, turbulent quantities are well predicted. Moreover, it also seems that the range of optimal ϵ/h ratios is the same for all turbulent statistics analyzed. This suggest that, although results show a high dependence on the filter length chosen, the

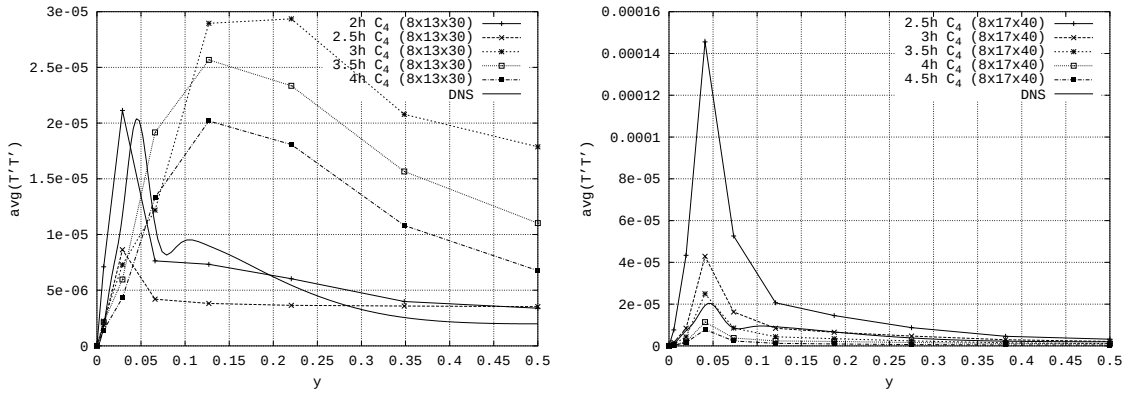

Figure 12: $\overline{T'T'}$ profile at the horizontal mid-height plane for different ϵ/h ratios. Left: $8 \times 13 \times 30$ simulations. Right: $8 \times 17 \times 40$ simulations

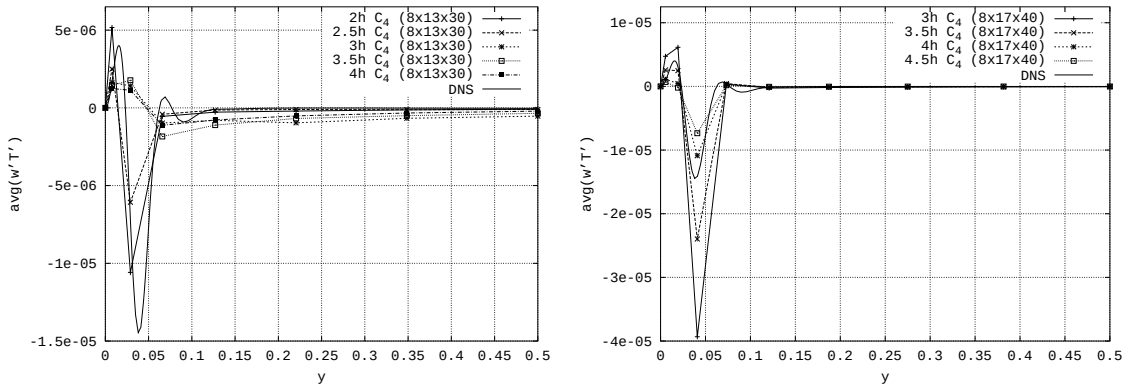

Figure 13: $\overline{u_3'T'}$ profile at the horizontal mid-height plane for different filter lengths ϵ. Left: $8 \times 13 \times 30$ simulations. Right: $8 \times 17 \times 40$ simulations

symmetry-preserving regularization models possess the ability to predict correctly the turbulent statistics.

4 CONCLUDING REMARKS

The performance of the symmetry-preserving regularization model C_4 has been tested for a $3D$ air-filled differentially heated cavity of aspect ratio 4 and $Ra = 10^{10}$ by means of direct comparison with the DNS results [5]. To do so, we have considered two coarse meshes consisting of $8 \times 13 \times 30$ and $8 \times 17 \times 40$ grid points, respectively, for different values of the ϵ/h ratio.

Comparison with DNS reference results show significant improvements in capturing the general pattern of the flow even for very coarse meshes. A fairly good agreement with the DNS mean flow is observed for a wide range of filter lengths. For turbulent statistics, although they are only fairly well predicted for a short range of ϵ/h ratios, the smoothed solutions exhibit the ability to capture the basic patterns of turbulent statistics and in the

worst cases they, at least, substantially improve the non-smoothed solution. This results suggest that the symmetry-preserving regularization models possess the ability to predict correctly also turbulent statistics.

In conclusion, considering the inherent difficulty of turbulence modelling, we consider that the these first results displayed here illustrate the great potential of symmetry-preserving smoothing method as a simulation shortcut for a differentially heated cavity. Moreover, since no *ad hoc* phenomenological arguments that can not be formally derived from the governing Navier-Stokes equations are used it suggest that this method may be valid for any other configuration. Nevertheless, simulations for a wide variety of cases and meshes will be necessary to confirm these preliminary conclusions.

REFERENCES

[1] A. Sergent, P. Joubert and P. Le Quéré, Development of a local subgrid diffusivity model for large-eddy simulation of buoyancy-driven flows: application to a square differentially heated cavity,*Numerical Heat Transfer, part A*, **44**, 8, 789–810, (2003).

[2] K. J. Hsieh and F. S. Lien, Numerical modeling of buoyancy-driven turbulent flows in enclosures, *International Journal of Heat and Fluid Flow*, **25**, 659–670, (2004).

[3] S. Kenjereš, S. B. Gunarjo and K. Hanjalić, Contribution to elliptic relaxation modelling of turbulent natural and mixed ceonvection, *International Journal of Heat and Fluid Flow*, **26**, 569–586, (2005).

[4] M. Soria, F. X. Trias, C. D. Pérez-Segarra and A. Oliva, Direct numerical simulation of a three-dimensional natural-convection flow in a differentially heated cavity of aspect ratio 4, *Numerical Heat Transfer, part A*, **45**, 649–673, (2004).

[5] F. X. Trias, M. Soria, A. Oliva and C. D. Pérez-Segarra. Direct numerical simulations of two- and three-dimensional turbulent natural convection flows in a differentially heated cavity of aspect ratio 4, *Journal of Fluid Mechanics*, submitted.

[6] J. Leray. Sur le movement d'un liquide visqueux emplissant l'espace. *Acta Math.*, **63**, 193–248, (1934).

[7] C. Foias, D.D. Holm and E.S. Titi. The Navier-Stokes-alpha model of fluid turbulence. *Physica D*, **152**, 505–519, (2001).

[8] B.J. Geurts and D.D. Holm. Regularization modeling for large-eddy simulation. *Phys. Fluids*, **15**, L13-L16, (2003).

[9] J.L. Guermond, J.T. Oden and S. Prudhomme. Mathematical perspectives on large eddy simulation models for turbulent flows. *J. Math. Fluid. Mech.*, **6**, 194-248, (2004).

[10] C. Foias, O. Manley, R. Rosa and R. Temam. *Navier-Stokes Equations and Turbulence*, Cambridge University Press, (2001).

[11] J. Vukadinovic. Density of global trajectories for filtered Navier-Stokes equations. *Nonlinearity*, **17**, 953–974, (2004).

[12] D. Carati, G.S. Winckelmans and H. Jeanmart. Exact expansions for filtered-scales modelling with a wide class of LES filters. In: P. Voke *et al.* (eds.) *Direct and Large-Eddy Simulation III*, Kluwer, 213–224,(1999).

[13] A.J. Chorin and J.E. Marsden. *A Mathematical Introduction to Fluid Mechanics*, Springer, (1979).

[14] J.H. Ferziger. Direct and large eddy simulation of turbulence. In: A. Vincent (ed.) *Numerical Methods in Fluid Dynamics*, American Mathematical Society, (1998).

[15] R.W.C.P. Verstappen and A.E.P. Veldman. Symmetry-preserving discretization of turbulent flow. *J. Comp. Phys.*, **187**, 343-368, (2003).